First publ. in: Physical Review B 68 (2003), 45414

Preparation, structure, and electronic properties of Fe_3O_4 films on the $Fe(110)/Mo(110)/Al_2O_3(11\bar{2}0)$ substrate

M. Fonin,[1] Yu. S. Dedkov,[1] J. Mayer,[2] U. Rüdiger,[1,3] and G. Güntherodt[1]
[1]*II. Physikalisches Institut, Rheinisch-Westfälische Technische Hochschule Aachen, 52056 Aachen, Germany*
[2]*Gemeinschaftslabor für Elektronenmikroskopie, Rheinisch-Westfälische Technische Hochschule Aachen, 52056 Aachen, Germany*
[3]*Fachbereich Physik, Universität Konstanz, 78457, Konstanz, Germany*

The surface and interface structure as well as the electronic properties of thin epitaxial $Fe_3O_4(111)$ films prepared by *in situ* oxidation of thin Fe(110) films grown on $Al_2O_3(11\bar{2}0)$ substrates using a Mo(110) buffer layer were investigated by low-energy electron diffraction (LEED), scanning tunneling microscopy (STM), transmission electron microscopy (TEM), and spin-polarized angle-resolved photoemission spectroscopy (SPARPES). The annealing of Fe(110) films at 700 °C in an O_2 atmosphere leads to the formation of epitaxial $Fe_3O_4(111)$ films. Atomically resolved STM images of the $Fe_3O_4(111)$ surface show a hexagonal symmetry with 6 Å periodicity. Well-controlled interface properties at the $Fe_3O_4(111)/Fe(110)$ and Fe(110)/Mo(110) interfaces were confirmed by TEM. A high spin polarization value of about $-(60\pm5)\%$ was found near the Fermi energy E_F at room temperature by means of SPARPES with a photon energy of $h\nu=21.2$ eV. The electronic structure and spin polarization are compared to the corresponding values recently found on epitaxial $Fe_3O_4(111)$ films grown on W(110) single-crystal substrates.

PACS number(s): 68.55.−a, 68.35.−p, 68.37.−d

I. INTRODUCTION

Investigations of magnetic multilayered thin-film systems exhibiting giant magnetoresistance[1,2] (GMR) and tunnel magnetoresistance[3,4] (TMR) have developed rapidly in recent years. Spin-dependent electron transport phenomena in magnetic tunnel junctions (MTJ's) make these multilayers attractive for possible applications as magnetic field sensors[5,6] and nonvolatile magnetic random access memory (MRAM) devices.[4,7,8]

According to Jullière's model,[9] the TMR of ferromagnet/insulator/ferromagnet tunnel junctions depends on the spin polarization of the ferromagnetic electrodes used. The TMR increases with an increasing spin polarization of the electrode materials. The theoretically predicted 100% spin polarization at the Fermi level E_F of Fe_3O_4,[10] CrO_2,[11] and NiMnSb [12] makes these so-called half-metallic ferromagnets (HMF's) promising materials for various magnetoelectronic devices.

Theoretical calculations of the density of states (DOS) of magnetite (Fe_3O_4) predict only minority spin states at the E_F (Ref. 10). Spin-resolved photoelectron yield measurements performed on single-crystalline Fe_3O_4 samples showed a large spin polarization of -60% near the photothreshold.[13] Recently, the possible half-metallic ferromagnetic nature of epitaxial $Fe_3O_4(111)$ thin films grown on Fe(110)/W(110) was experimentally confirmed by means of spin- and angle-resolved photoemission spectroscopy (SPARPES). In this experiment a negative spin polarization of $-(80\pm5)\%$ at E_F was measured at room temperature.[14]

The scientific and technological importance of oxidic HMF's has motivated a large number of experimental investigations concerning their structural and magnetic properties in the bulk state as well as in thin films.[15–28] Epitaxial Fe_3O_4 films were grown using different techniques on a variety of substrates, including Fe(110),[15,16] Pt(111),[17–19] W(110),[14,20] MgO(100),[21–26] $MgAl_2O_4(100)$,[27] $SrTiO_3(100)$,[27,28] and $Al_2O_3(0001)$.[28] Nevertheless, the study of the surface and interface structure of well-ordered Fe_3O_4 thin films on insulating substrates and resulting electronic properties is still a very important and complex issue, which is critical for the investigation of spin-polarized transport phenomena in complex multilayered structures based on highly spin-polarized $Fe_3O_4(111)$ electrodes.

In this article we report on a careful oxidation study of 200 Å thick epitaxial Fe(110) films grown on $Al_2O_3(11\bar{2}0)$ substrates using Mo(110) seed layers. The possibility of a smooth growth of Fe(110) films on Mo(110) seed layers was demonstrated before,[29,30] and the growth mechanism was discussed in detail.[31] In this case smooth epitaxial Fe(110) films were obtained by the growth at room temperature with a subsequent annealing procedure at 500 °C. The oxidation of the Fe(110) films was performed by annealing at 700 °C in an O_2 gas atmosphere. Low-energy electron diffraction (LEED) patterns show a clear transition from a Fe(110) to a $Fe_3O_4(111)$ surface. A well-defined $Fe_3O_4(111)$ surface was also confirmed by scanning tunneling microscopy (STM). Atomically resolved images of the $Fe_3O_4(111)$ surface show a hexagonal atomic structure with 6 Å periodicity. Sharp $Fe_3O_4(111)/Fe(110)$ and Fe(110)/Mo(110) interfaces without intermixing were found by transmission electron microscopy (TEM). The spin-dependent electronic structure of the $Fe_3O_4(111)$ films was investigated at room temperature by means of SPARPES. Near E_F a negative spin polarization of up to $-(60\pm5)\%$ was found. This value of spin polarization at E_F was found to be lower compared to previous studies on thin epitaxial $Fe_3O_4(111)$ films grown on single-crystal W(110) substrates applying the same growth technique.

II. EXPERIMENT

The thin-film growth and the surface characterization were carried out in an ultrahigh-vacuum (UHV) system with a base pressure of 8×10^{-11} mbar equipped with an electron-beam evaporator (Omicron EFM3T) for thin-film deposition, LEED optics, and a STM (Omicron UHV AFM/STM). All STM measurements were carried out at room temperature using electrochemically etched polycrystalline tungsten tips cleaned in UHV by Ar^+ sputtering. The presented STM images were taken in the constant-current mode.

The TEM characterization of the layered system was performed on an analytical TEM with a field emission gun (FEI TECNAI F20) equipped with an energy dispersive x-ray (EDX) detector and a post-column imaging filter (GATAN GIF). The TEM specimens were prepared using standard cross-sectioning techniques with a final Ar^+ ion thinning at 3 keV ion energy.

The photoemission experiments were done at room temperature in a separate UHV system (base pressure 1×10^{-10} mbar) for angle-resolved photoemission spectroscopy with spin analysis described in detail in Ref. 32. The unpolarized He I ($h\nu=21.2$ eV) resonance line was used for the photoemission experiments. The spin-resolved photoemission spectra have been recorded in normal emission by a 180° hemispherical energy analyzer connected to a 100 kV Mott detector for spin analysis. The energy resolution was 100 meV and the angle resolution ±3°. The spin-resolved measurements have been performed in magnetic remanence after having applied a magnetic field pulse of about 500 Oe along the in-plane $\langle 11\bar{2}\rangle$ easy magnetic axis of the thin $Fe_3O_4(111)$ films, which is perpendicular to the easy magnetic axis of the Fe(110) film. In this case the influence of the Fe(110) underlayer on the spin polarization value can be excluded.

The $Al_2O_3(11\bar{2}0)$ substrates were of rectangular shape (10×5 mm^2) cut with the long edges 35° off the in-plane [0001] direction in order to align the [001] easy magnetic axis of the (110)-oriented Fe films along these edges of the substrate.[30] The substrates were cleaned in acetone, isopropanol, and methanol before the introduction into UHV and finally annealed *in situ* for 2 h at 650 °C. The metals (Mo and Fe) were deposited from 2 mm thick rods heated by electron bombardment with a growth rate of about 1 monolayer (ML)/min. The substrate temperature during the Mo deposition was kept at 700 °C. The temperature was monitored by a Chromel-Alumel thermocouple on the sample holder. The absolute accuracy of the temperature measurements was ±20 °C. The Fe surface oxidation was done by exposing the film to high-purity O_2 gas using a variable-leak valve followed by an annealing procedure. Oxygen doses were determined from an ion-gauge reading without any additional correction for oxygen. After the sample preparation in the thin-film deposition system the films were transferred into the photoemission spectroscopy (PES) chamber by breaking the UHV conditions. After the introduction into the PES chamber the sample surface was cleaned by Ar^+ sputtering under grazing angle ($E=500$ eV, $p=1\times10^{-6}$ mbar) for 10 min followed by an annealing step in 5×10^{-6} mbar O_2 atmosphere at 500 °C for 30 min.

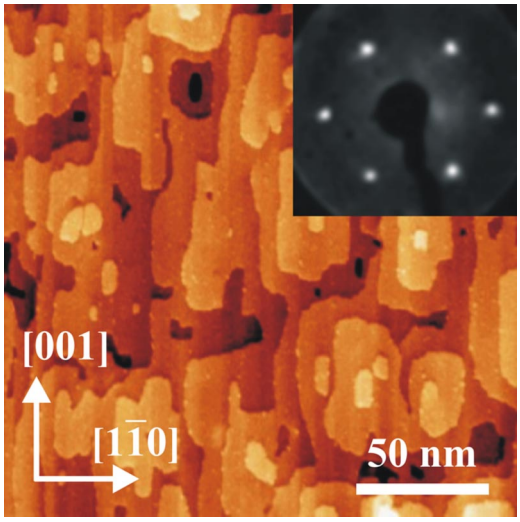

FIG. 1. STM image of a 100 Å thick Mo(110) film grown on an $Al_2O_3(11\bar{2}0)$ substrate at 700 °C (200×200 nm^2). The image was acquired with a tunneling current (I_T) of 0.12 nA and a tunneling voltage (U_T) +1 V. The inset shows a LEED pattern of the same film. The energy of the primary beam was 137 eV.

III. RESULTS AND DISCUSSION

Figure 1 shows a STM image of a 100 Å thick Mo(110) film grown on an $Al_2O_3(11\bar{2}0)$ substrate at 700 °C. A characteristic monoatomic step morphology with a step height of 2.19 Å is visible in this image. The shape of the small rectangular islands shows an anisotropic in-plane growth mode of Mo terraces. The long axis of the islands and the steps are preferentially oriented parallel to the [001] direction of the (110) bcc plane. On a scale of 200×200 nm^2 approximately 10 open layers of Mo(110) are visible, indicating the existence of an effective step-edge barrier (Schwoebel-Ehrlich barrier[33]) preventing a complete interlayer mass transport during the growth. The inset in Fig. 1 shows a (1×1) LEED pattern of an epitaxially grown Mo(110) film. The LEED image with a twofold symmetry is typical for the bcc Mo(110) surface.

The growth of epitaxial Fe(110) films on a 100 Å thick Mo(110) seed layer which was deposited on a $Al_2O_3(11\bar{2}0)$ substrate was performed at room temperature. Afterwards, the 200 Å thick Fe(110) films were annealed at 500 °C for 1 h to improve the surface structure of the films. Figure 2 shows a 200×200 nm^2 STM image of a 200 Å thick Fe(110) film on a $Mo(110)/Al_2O_3(11\bar{2}0)$ surface. The height of monoatomic steps present in this image are 2.05 Å with the step edges preferably directed along the Fe [001] axis, which can be induced by a slight miscut of the $Al_2O_3(11\bar{2}0)$ substrate. The vertical peak-to-peak roughness of the Fe(110) film on a scale of 1000×1000 nm^2 is not more than 20 Å. Very sharp (1×1) LEED patterns of the bcc Fe(110) surface without any side reflexes[31,34] have been observed as shown in the inset of Fig. 2. Some dislocations can be found on the

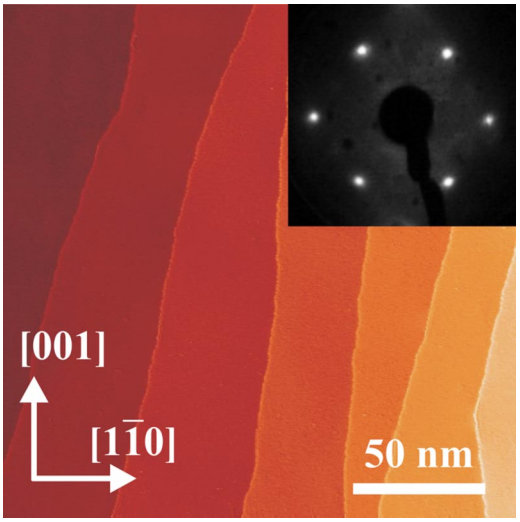

FIG. 2. STM image of a 200 Å thick Fe (110) film deposited on the Mo(110)/$Al_2O_3(11\bar{2}0)$ system at room temperature and subsequently annealed at 500 °C (200×200 nm^2). The image was acquired with a tunneling current (I_T) of 0.12 nA and a tunneling voltage (U_T)+1 V. The inset shows a LEED pattern of the same film. The energy of the primary beam was 172 eV.

atomically flat Fe planes (not shown here). These dislocations can be attributed to anisotropic strain relaxation processes on the surface during the growth and annealing of the Fe(110) film.

In the next step the epitaxial Fe(110) films were oxidized by annealing in 5×10^{-6} mbar O_2 at 700 °C for 30 min. The surface morphology of the resulting $Fe_3O_4(111)$ film was studied by STM and is shown in Fig. 3. Large hexagonally shaped islands with a lateral extension of more than 100 nm have been formed [see Fig. 3(a)]. The longer side edges of the islands are oriented along the in-plane $[\bar{1}10]$, $[01\bar{1}]$, and $[10\bar{1}]$ crystallographic directions of the $Fe_3O_4(111)$ surface. The islands are monoatomically flat with step heights of approximately 5 Å, which corresponds to the distance between equivalent $Fe_3O_4(111)$ surface terminations.[18] The vertical peak-to-peak roughness of the surface on a lateral scale of 1000 nm is about 60 Å.

Magnetite (Fe_3O_4) has a cubic inverse spinel structure. Oxygen anions form a close-packed fcc lattice with tetrahedrally (*A* sites) and octahedrally (*B* sites) coordinated Fe^{2+} and Fe^{3+} cations located in the interstitial sites. The structure can be also considered as hexagonal close-packed oxygen (111) layers forming a cubic *ABCABC*… stacking sequence along the [111] direction with planes of the tetrahedrally and octahedrally coordinated Fe atoms in between. The $Fe_3O_4(111)$ two-dimensional unit cell has a lattice constant of 5.92 Å. Defining the atomic density of the close-packed oxygen layer as 1 ML, six ideal bulk terminations can be obtained: 1/4 ML of Fe_{tet1} or Fe_{tet2} atoms, 3/4 ML of Fe_{oct1} or Fe_{oct2} atoms, or close-packed O_1 or O_2 layers, with a distance of 4.85 Å between equivalent terminations.[18]

Figure 3(b) shows a STM image with atomic resolution of the regular $Fe_3O_4(111)$ surface. A hexagonal lattice with a 6 Å periodicity and a corrugation amplitude of about 0.5 Å can

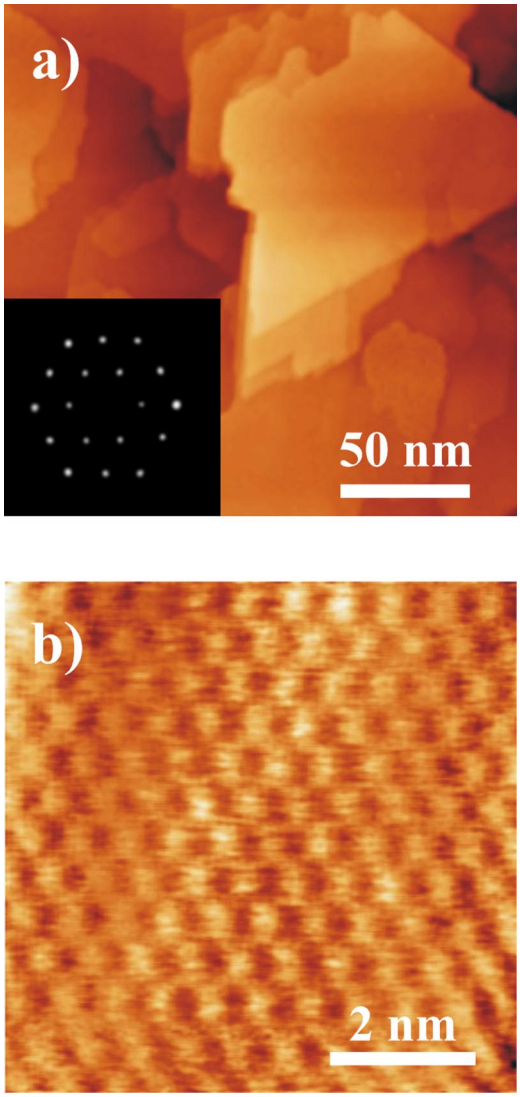

FIG. 3. STM image of a well-ordered $Fe_3O_4(111)$ film on Fe(110)/Mo(110)/$Al_2O_3(11\bar{2}0)$ obtained by annealing the sample at 700 °C in 5×10^{-6} mbar oxygen (O_2): (a) a 200×200 mm^2 surface section and (b) an atomically resolved regular $Fe_3O_4(111)$ surface (7×7 nm^2). The images were acquired with a tunneling current (I_T) of 0.12 nA and a tunneling voltage (U_T)+1 V. The inset in (a) shows a hexagonal (2×2) LEED pattern of the same film. The energy of the primary beam was 121 eV.

be clearly seen in this image. The same characteristic hexagonal lattice is observed for both positive and negative tunneling bias voltages between +1 and −1 V without significant changes in the image contrast. This value is in good agreement with the $Fe_3O_4(111)$ in-plane lattice constant of 5.92 Å. The $Fe_3O_4(111)$ surface structure determined by LEED [see inset in Fig. 3(a)] suggests that the bright spots observed by STM correspond to the positions of the Fe_{tet1} cations in the topmost layer, since they form the same hexagonal surface lattice with a 6 Å periodicity. This surface structure can be described as an unreconstructed bulk termination of $Fe_3O_4(111)$ with a 1/4 ML of Fe_{tet1} atoms over a close-packed oxygen layer underneath, which is in a good agreement with the previous studies of comparable

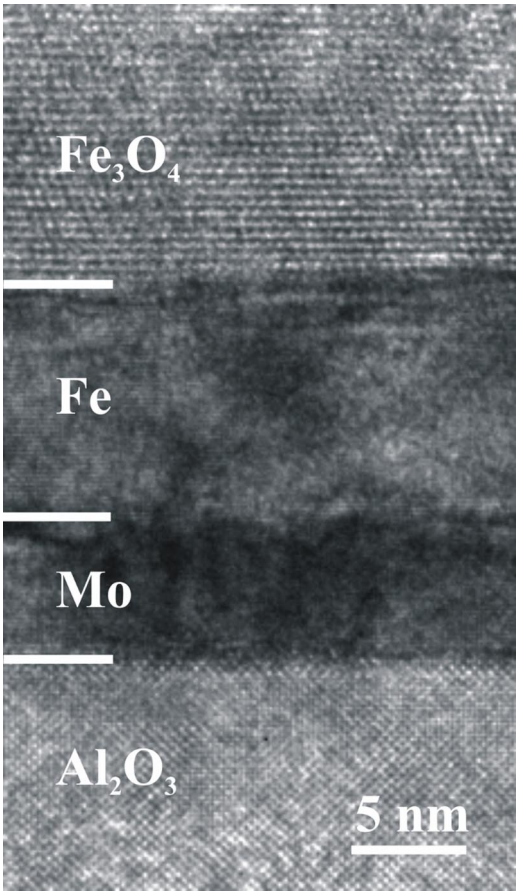

FIG. 4. TEM cross-section micrograph of the $Fe_3O_4(111)/Fe(110)/Mo(110)/Al_2O_3(11\bar{2}0)$ system imaged along the zone axes given in Table I. White lines indicate the individual interfaces between different layers.

$Fe_3O_4(111)/Pt(111)$ surfaces.[16,17]

Figure 4 shows a cross-section TEM image of the $Fe_3O_4(111)/Fe(110)/Mo(110)/Al_2O_3(11\bar{2}0)$ system. Lattice planes are resolved in all three layers of the system and in the sapphire substrate. The interfaces between all four materials are clearly visible and abrupt for the $Mo(110)/Al_2O_3(11\bar{2}0)$ and $Fe_3O_4(111)/Fe(110)$ interfaces, at which only steps with monolayer height can be observed. The interface between Mo and Fe is less clearly visible in Fig. 4: however, the chemical analysis performed with the energy filter revealed that it is chemically sharp within the given resolution limit (about 2 nm). No indication for interdiffusion has been found at all three interfaces. To emphasize this a high-resolution image of the Al_2O_3/Mo interface imaged along the $[1\bar{1}01]$ Al_2O_3 and [001] Mo zone axes is depicted in Fig. 5. A diffraction pattern verifying the epitaxial orientation relationship for all four materials is shown in Fig. 6 together with a schematic drawing indicating the positions of the reflections caused by the four lattices with the incident beam direction along the zone axes given in Table I. It is interesting to note that Fe_3O_4 occurs in the two mirror-related twin variants which preserve the (111) interface plane and ⟨110⟩-type projection.

After preparation the $Fe_3O_4(111)$ samples were transferred from the thin-film deposition system into the PES chamber under air conditions for spin-resolved PES experiments. Directly after the *ex situ* transfer of the $Fe_3O_4(111)$ samples into the PES chamber the $Fe_3O_4(111)$ surface was cleaned by Ar^+ sputtering for 10 min under a grazing angle with a beam energy of $E=500$ eV and an Ar pressure of 1×10^{-6} mbar followed by annealing in a 5×10^{-6} mbar O_2 atmosphere at 500 °C for 30 min. The chemical analysis performed by Auger spectroscopy directly after the cleaning procedure did not reveal carbon or any other contaminations. The crystalline quality of the surface was preserved as confirmed by LEED.

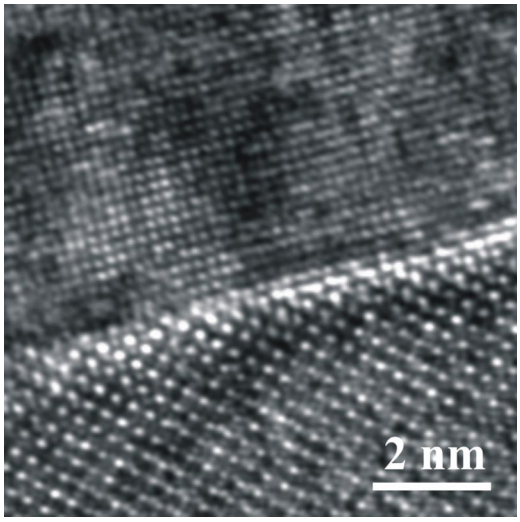

FIG. 5. High-resolution image of the Al_2O_3/Mo interface imaged along the $Al_2O_3(11\bar{2}0)$ $[1\bar{1}01]$ and Mo(110) [001] zone axes. The interface is atomically sharp, and contrast variations in the Mo lattice are caused by damage introduced during ion-beam thinning.

Figure 7 shows spin-resolved photoemission spectra recorded near E_F together with the total photoemission intensity (left-hand panel) and the resulting spin polarization (right-hand panel) as a function of the binding energy of $Fe_3O_4(111)$ films. In (a) the spectra of an $Fe_3O_4(111)$ layer on the Fe(110)/W(110) system are shown, which are taken from Ref. 14. In (b) the spectra of an $Fe_3O_4(111)$ layer on the $Fe(110)/Mo(110)/Al_2O_3(11\bar{2}0)$ system are presented. The open squares in (c) correspond to the spin polarization of the $Fe_3O_4(111)/Fe(110)/W(110)$ system taken from Ref. 14, and solid circles mark the spin polarization of the $Fe_3O_4(111)/Fe(110)/Mo(110)/Al_2O_3(11\bar{2}0)$ system. The features of Fe $3d$ bands in the range of 2 eV below E_F in the PES spectra of the $Fe_3O_4(111)$ film on the $Al_2O_3(11\bar{2}0)$ does not differ from the film on W(110), but a significant decrease of the Fe $3d$ photoemission intensity has been observed for the films grown on the $Al_2O_3(11\bar{2}0)$ substrate. A possible reason for this effect can be an increasing structural in-plane strain of the $Fe_3O_4(111)$ surface layers caused by lattice mismatch with the multilayered system grown on $Al_2O_3(11\bar{2}0)$ substrates. Another reason for the photoemission intensity decrease can be the cleaning procedure after the *ex situ* sample transfer into the PES chamber. As reported before,[35] the cleaning procedure can crucially

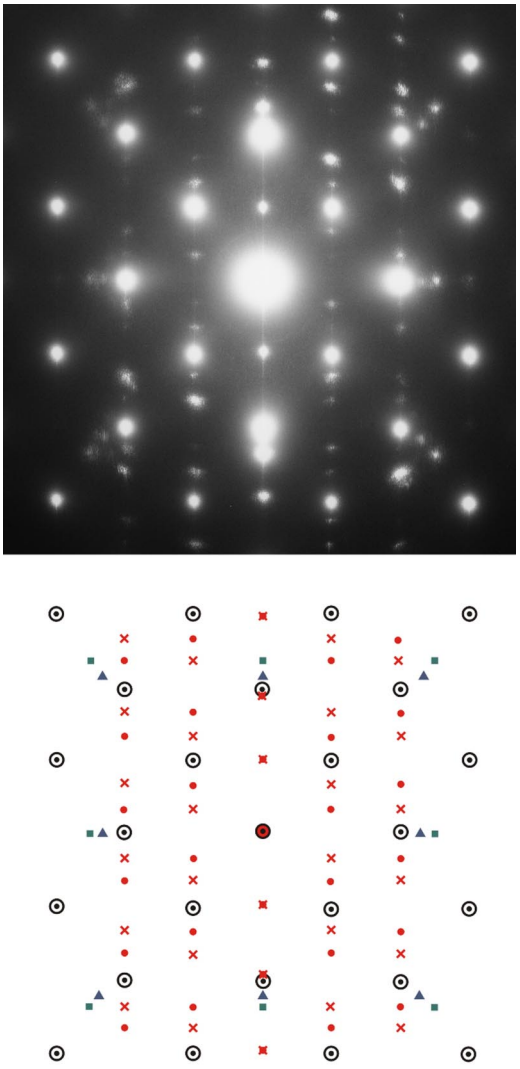

FIG. 6. TEM diffraction pattern showing the expected reflections of all four lattices in an orientation along the zone axes given in Table I. In the schematic drawing, large circles (⊙) denote reflections of Al_2O_3, triangles (▲) of Mo, squares (■) of Fe, dots (●), and crosses (×) denote reflections of the two mirror-related twin variants of Fe_3O_4.

influence the surface structure, leading to a decrease or total loss of the spin polarization.

The spin-resolved spectra of the valence band near E_F (Fig. 7) clearly show a dominant emission from the spin-down Fe $3d$ states ($\lesssim$1.5 eV) and the O $2p$ states ($\gtrsim$1.5 eV) (not shown here). The spin-resolved spectra exhibit a clear half-metallic feature: i.e., a metallic Fermi cutoff for the minority spin and a disappearance of spectral weight near E_F—reflecting the energy gap—for the majority spin. The $Fe_3O_4(111)$ films on the $Al_2O_3(11\bar{2}0)$ substrates show a maximum negative spin polarization at E_F of about $-(60 \pm 5)\%$ at room temperature. However, this polarization value cannot be related to a contribution from Fe(110) underlayer, as the thickness of the $Fe_3O_4(111)$ film determined by TEM (Fig. 4) is about 150 Å. Comparing the $Fe_3O_4(111)$

TABLE I. The epitaxial layer system can be characterized by the interface planes and one set of zone axes which align parallel in the interface plane for each of the four materials. The given zone axes are also parallel to the viewing direction of the TEM micrographs in Figs. 4 and 5 as well as of the TEM diffraction pattern in Fig. 6. Note that the Fe_3O_4 lattice occurs in two mirror-related twin variants.

	Interface plane	In-plane zone axis
Al_2O_3	$(11\bar{2}0)$	$[1\bar{1}01]$
Mo	(110)	[001]
Fe	(110)	[001]
Fe_3O_4	(111)	$[1\bar{1}0]$,$[\bar{1}10]$

films on W(110) and $Al_2O_3(11\bar{2}0)$ substrates, the reduction of the observed spin polarization for the $Fe_3O_4(111)$ films on the $Al_2O_3(11\bar{2}0)$ substrate may be caused by the cleaning procedure or by strain in the $Fe_3O_4(111)$ surface layers caused by a lattice mismatch between the Mo(110) and Fe(110) layers as well as Fe(110) and $Fe_3O_4(111)$ layers. As reported by Jeng and Guo, resulting strain can lead to a reduction of the spin polarization value.[36] In this case the presence of uniaxial strain leads to a broadening of the *B*-site Fe $3d$ bands, reducing the insulating band gap of the majority

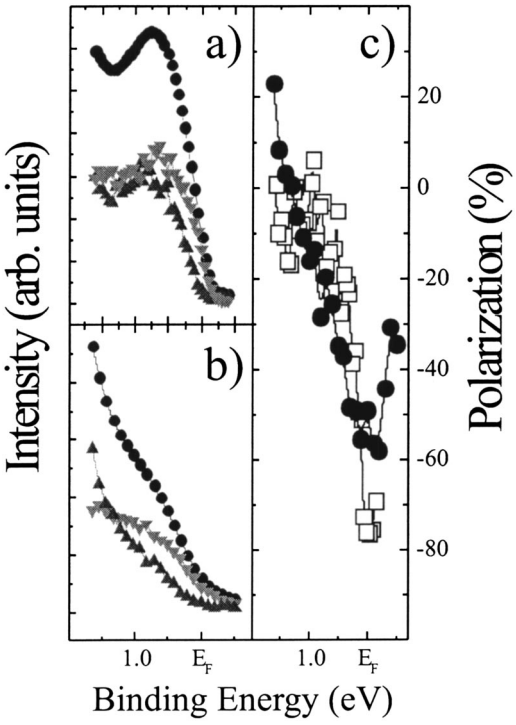

FIG. 7. Left-hand panel: spin-resolved photoemission spectra of (a) the $Fe_3O_4(111)$/Fe(110)/W(110) system and of (b) the $Fe_3O_4(111)$/Fe(110)/Mo(110)/$Al_2O_3(11\bar{2}0)$ system for $h\nu = 21.2$ eV in normal emission. The lines through the data points have been obtained by a three-point averaging FFT (fast Fourier transformation) smoothening procedure. Right-hand panel (c): spin polarization as function of binding energy: Open squares: the $Fe_3O_4(111)$/Fe(110)/W(110) system. Solid circles: the $Fe_3O_4(111)$/Fe(110)/Mo(110)/$Al_2O_3(11\bar{2}0)$ system.

spin. As a consequence, the half-metallic behavior of cubic magnetite is reduced and in high-strain regimes $Fe_3O_4(111)$ can eventually turn into normal metal behavior.

IV. CONCLUSION

Epitaxial 200 Å thick Fe(110) films were grown on $Al_2O_3(11\bar{2}0)$ substrates using a 100 Å thick Mo(110) seed layer. The *in situ* oxidation of the Fe(110) films by annealing in O_2 (5×10^{-6} mbar) at 700 °C for 30 min leads to epitaxial $Fe_3O_4(111)$ films. Atomically resolved STM images of the $Fe_3O_4(111)$ surface show a hexagonal in-plane symmetry with 6 Å periodicity. The epitaxial relationship with well-controlled, chemically abrupt interfaces between all layers could be confirmed in the $Fe_3O_4(111)/Fe(110)/Mo(110)/Al_2O_3(11\bar{2}0)$ system by high-resolution and analytical TEM as well as by electron diffraction. A reduced spin polarization value of about $-(60\pm5)\%$ was found near E_F at room temperature for the $Fe_3O_4(111)$ films on $Al_2O_3(11\bar{2}0)$ substrates compared to $-(80\pm5)\%$ for $Fe_3O_4(111)$ films on W(110) single crystal.

ACKNOWLEDGMENTS

This work was supported by the German Federal Ministry of Education and Research (BMBF) under Grant Nos. FKZ 05KS1PAA/7 and FKZ 13N7988. The authors would like to thank C. Herwartz and T. E. Weirich for help with the TEM experiments.

[1] M. N. Baibich, J. M. Broto, A. Fert, F. Nguyen Van Dau, F. Petroff, P. Etienne, G. Creuzet, A. Friederich, and J. Chazelas, Phys. Rev. Lett. **61**, 2472 (1988).
[2] G. Binasch, P. Grünberg, F. Saurenbach, and W. Zinn, Phys. Rev. B **39**, 4828 (1989).
[3] J. S. Moodera, L. R. Kinder, T. M. Wong, and R. Merservey, Phys. Rev. Lett. **74**, 3273 (1995).
[4] W. J. Gallagher *et al.*, J. Appl. Phys. **81**, 3741 (1997).
[5] M. Sato, H. Kikuchi, and K. Kobayashi, J. Appl. Phys. **83**, 6691 (1998).
[6] M. Tondra, J. M. Daughton, D. Wang, R. S. Beech, A. Fink, and J. A. Taylor, J. Appl. Phys. **83**, 6688 (1998).
[7] J. M. Daughton, J. Appl. Phys. **81**, 3758 (1997).
[8] H. Boeve, R. J. M. van der Veerdonk, B. Dutta, J. de Boeck, J. S. Moodera, and G. Borghs, J. Appl. Phys. **83**, 6700 (1998).
[9] M. Jullière, Phys. Lett. **54A**, 225 (1975).
[10] Z. Zhang and S. Satpathy, Phys. Rev. B **44**, 13 319 (1991).
[11] K.-H. Schwarz, J. Phys. F: Met. Phys. **16**, L211 (1986); M. A. Korotin, V. I. Anisimov, D. I. Khomskii, and G. A. Sawatzky, Phys. Rev. Lett. **80**, 4305 (1998).
[12] R. A. de Groot, F. M. Müller, P. G. van Engen, and K. H. J. Buschow, Phys. Rev. Lett. **50**, 2024 (1983).
[13] S. F. Alvarado, W. Eib, F. Meier, D. T. Pierce, K. Sattler, H. C. Siegmann, and J. P. Remeika, Phys. Rev. Lett. **34**, 319 (1975); S. F. Alvarado, M. Erbudak, and P. Munz, Phys. Rev. B **14**, 2740 (1976).
[14] Yu. S. Dedkov, U. Rüdiger, and G. Güntherodt, Phys. Rev. B **65**, 064417 (2002).
[15] V. S. Smentkowsky and J. T. Yates, Surf. Sci. **232**, 113 (1990).
[16] A. Wight, N. G. Condon, F. M. Leibsle, G. Worthy, and A. Hodgson, Surf. Sci. **331–333**, 133 (1995).
[17] W. Weiss, A. Barbieri, M. A. Van Hove, and G. A. Somorjai, Phys. Rev. Lett. **71**, 1848 (1993).
[18] M. Ritter and W. Weiss, Surf. Sci. **432**, 81 (1999); W. Weiss and M. Ritter, Phys. Rev. B **59**, 5201 (1999).
[19] Sh. K. Shaikhutdinov, M. Ritter, X. G. Wang, H. Over, and W. Weiss, Phys. Rev. B **60**, 11 062 (1999).
[20] H.-J. Kim, J.-H. Park, and E. Vescovo, Phys. Rev. B **61**, 15 284 (2000); **61**, 15 288 (2000).
[21] G. M. Gaines, P. J. H. Bloemen, J. T. Kohlhepp, C. W. T. Bulle-Lieuwma, R. M. Wolf, A. Reinders, R. M. Jungblut, P. A. A. van der Heijden, J. T. W. M. van Eemeren, J. aan de Stegge, and W. J. M. de Jonge, Surf. Sci. **373**, 85 (1997).
[22] J. F. Anderson, M. Kuhn, and U. Diebold, Phys. Rev. B **56**, 9902 (1997).
[23] F. C. Voogt, T. Fujii, P. J. M. Smulders, L. Niesen, M. A. James, and T. Hibma, Phys. Rev. B **60**, 11 193 (1999).
[24] T. Fujii, F. M. F. de Groot, G. A. Sawatzki, F. C. Voogt, T. Hibma, and K. Okada, Phys. Rev. B **59**, 3195 (1999).
[25] Y. J. Kim, Y. Gao, and S. A. Chambers, Surf. Sci. **371**, 358 (1997).
[26] S. A. Chambers, S. Thevuthasan, and S. A. Joyce, Surf. Sci. Lett. **450**, L273 (2000).
[27] W. F. J. Fontijn, R. M. Wolf, R. Metselaar, and P. J. van der Zaag, Thin Solid Films **292**, 270 (1997).
[28] S. B. Ogale, K. Ghosh, R. P. Sharma, R. L. Greene, R. Ramesh, and T. Venkatesan, Phys. Rev. B **57**, 7823 (1998).
[29] B. M. Clemens, R. Osgood, A. P. Payne, B. M. Lairson, S. Brennan, R. L. White, and W. D. Nix, J. Magn. Magn. Mater. **121**, 37 (1993).
[30] J. Yu, U. Rüdiger, A. Kent, L. Thomas, and S. S. P. Parkin, Phys. Rev. B **60**, 7352 (1999).
[31] U. May, R. Calarco, J. O. Hauch, H. Kittur, M. Fonine, U. Rüdiger, and G. Güntherodt, Surf. Sci. **489**, 144 (2001).
[32] R. Raue, H. Hopster, and E. Kisker, Rev. Sci. Instrum. **55**, 383 (1984).
[33] R. L. Schwoebel, J. Appl. Phys. **40**, 614 (1969).
[34] M. Tikhov and E. Bauer, Surf. Sci. **232**, 73 (1990).
[35] S. A. Morton, G. D. Waddill, S. Kim, Ivan K. Schuller, S. A. Chambers, and J. G. Tobin, Surf. Sci. Lett. **513**, L451 (2002).
[36] H.-T. Jeng and G. Y. Guo, Phys. Rev. B **65**, 094429 (2002).